IET Renewable Power Generation

Special Issue: Selected papers from the 7th International Conference on Clean Electrical Power (ICCEP 2019)

IET Journals
The Institution of Engineering and Technology

Design of GEMSTAR tidal current fixed pitch rotor controlled through a Permanent Magnet Generator (PMG) de-fluxing technique

ISSN 1752-1416
Received on 21st April 2020
Revised 8th October 2020
Accepted on 13th October 2020
E-First on 20th November 2020
doi: 10.1049/iet-rpg.2020.0434
www.ietdl.org

Domenico P. Coiro[1] ✉, Giancarlo Troise[2], Nadia Bizzarrini[2], Guido Lazzerini[1], Luigi Pio Di Noia[3], Diego Iannuzzi[3], Marino Coppola[3]

[1]*Department of Industrial Engineering, University of Naples Federico II, Via Claudio 21, 80125 Napoli, Italy*
[2]*Seapowerscrl, Via Claudio 21, 80125 Napoli, Italy*
[3]*Department of Electrical Engineering, University of Naples Federico II, Via Claudio 21, 80125 Napoli, Italy*
✉ *E-mail: domenico.coiro@unina.it*

Abstract: This work reports a study on a tidal current system named GEMSTAR, composed of two hydrokinetic turbines supported by a floating submerged structure. A flexible mooring cable links the floating support to the seabed allowing the free rotation of the system and its alignment to changing current direction. The work is mainly focused on the design of the turbine blade with two objectives: keeping a constant power output above the rated power condition and limiting the thrust increase between rated and maximum operating speed. A fixed pitch blade was considered, in order to reduce the costs associated to a complex pitch control mechanism. An analytical procedure for blade design is proposed and validated by comparison to other numerical methods. Above the rated current speed, the power is held constant while the rotational speed of the turbine and of the generator increases, assuming an over-speeding control strategy. The adopted design configuration relies on the possibility of the generator to operate in de-fluxing working conditions. As reported in the last part of this study, a numerical model of the generator has also been developed and applied to a test case in order to analyse the electric behaviour of the system.

Nomenclature

ρ	density, kg/m^3
v	axial velocity, m/s
a	axial induction, dimensionless
a'	rotational induction, dimensionless
N	number of blades, dimensionless
c	section chord, m
v_{rel}	relative velocity, m/s
ω	rotational velocity, rad/s
C_{d}	sectional drag coefficient, dimensionless
C_{l}	sectional lift coefficient, dimensionless
C_{N}	normal force coefficient, dimensionless
C_{H}	horizontal force coefficient, dimensionless
r	section radius, m
R	rotor radius, m
dr	radius increment between sections, m
dT	thrust increment between sections, N
dP	power increment between sections, W
T	thrust, N
P	power, W
$P_{n,t}$	turbine rated power, W
α	angle of attack, deg
θ	sectional twist, deg
Φ	in-flow angle, deg
F_{h}	sectional hydrodynamic force, N/m
L	sectional lift, N/m
D	sectional drag, N/m
N	sectional normal force, N/m
H	sectional horizontal force, N/m
R_{s}	stator resistance, Ω
L_{s}	stator inductance, H
p	number of poles pairs
I_L	inverter current limit, A
i_d	direct-axis current, A
i_q	quadrature-axis current, A
v_d	direct-axis voltage, V
v_q	quadrature-axis voltage, V
J	generator moment of inertia, kg m^2
Φ_{r}	rotor flux, Wb
ω_{r}	electric generator mechanical speed, rad/s
θ_{r}	rotor angular position, rad
T_{r}	active torque, Nm
T_{e}	electric torque, Nm

1 Introduction

This paper refers to the development of GEMSTAR, a system for harnessing tidal current energy (*Generatore Elettrico Marino, Sustainable Tethered Advanced Rotors*). The system is composed of two hydrokinetic turbines mounted on an underwater floating support structure, linked to the seabed by means of a flexible mooring cable. The overall configuration of the system is shown in Fig. 1. There are a few differences between this system and the so-called 'first generation tidal energy converters', of which the main features are shown in comprehensive reviews and workshop reports as in [1]. One is the self-alignment property of the system to the tidal current direction, avoiding the need of an active yaw-control or multi-directional turbines. The cable allows the system to align to the current and to capture the tidal current energy in both directions of tide ('flood' and 'ebb' currents) with passive stability. The answer to this well-known characteristic of the tidal currents for several projects with seabed-fixed structures is that of using rotating nacelles (such as in the turbines from Atlantis [2]) or special design of turbines that allows operation in both directions (such as in Voith Hydro [3]). This special design inevitably leads to a loss in the maximum power coefficient and to a cost increase. Another peculiarity of the GEMSTAR, with respect to all the seabed fixed systems, is the capability of easy emersion, lowering the costs of maintenance. An attempt to create a more flexible tidal current energy harvester is developed by Orbital with their system O2 2 MW [4]. The turbines are mounted on bars connected to a supporting ship. This configuration allows a very easy maintenance and the most flexible positioning on-site of the system in an arbitrary direction. The clear disadvantage is the supporting boat

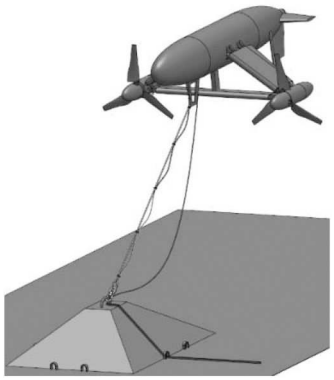

Fig. 1 *GEMSTAR system general arrangement view*

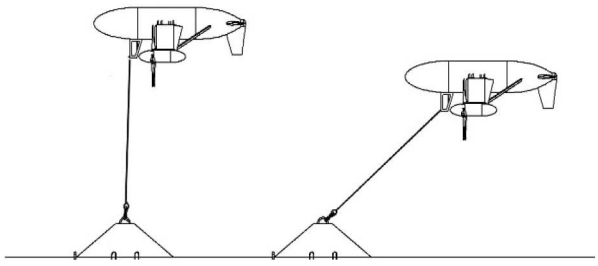

Fig. 2 *GEMSTAR system operating conditions: at rest (left), under water current action (right)*

itself, being subjected to sea-state, waves and ocean traffic. Thanks to the adjustable length of the linking cable, GEMSTAR can be positioned with a sufficient clearance from both extreme sea-state and wave interaction. It is worth remarking that Minesto Open Green [5] shares many of the advantages of GEMSTAR, such as the flexibility in handling the system outside water, the absence of active rotating control parts and the self-aligning properties, despite a very different concept of harvesting currents. In fact, this system exploits a self-generated motion of the entire system to induce the rotation of a downstream turbine. The motion of the entire system over a large underwater area limits the chance to install several units in the same area even though they state that the energy extraction is enhanced for the single unit. Furthermore, the adaptability to different sites is questionable due to the space required to operate the system. A similar project developed in Japan belong to Okinawa Institute of Science and Technology [6] where they investigated wave effects only on small-scale turbine behaviour and IHI-New Energy-NEDO [7] which has developed and tested a large-scale prototype in Kuroshio ocean current. Their aim is to harness energy from surface, low-speed, stable Kuroshio ocean current which, differently from tidal current, are one-directional.

The GEMSTAR has been developed in cooperation with University of Naples, continuing the previously developed GEM research project [8]. Earlier research activities comprise several test campaigns on the first prototype.

The system is designed to exploit the kinetic energy available in natural stream flows, according to a widely diffused and studied concept [9, 10]. Due to the considerable amount of energy resource theoretically available, tidal currents are particularly attractive. Some of the most interesting areas along the Italian coastline for marine current exploitation are located within the Strait of Messina [11].

The project is currently undergoing a design revision. In particular, the rotor configuration was reconsidered and the turbine blades were redesigned. Following a 'systemic approach' as it was done in [12], the novel turbine blade design method presented in this paper aims to improve the performance of the GEMSTAR configuration, searching for an optimised blade geometry at the design point while meeting the requirements of the fixed pitch – variable speed control strategy adopted for the generator coupling. In comparison to previous works, the paper presents an alternative approach to the blade aerodynamic design, developing a design procedure based on the blade element theory and adjusted for the specific issues of coupling the fixed-pitch configuration and the de-fluxing control strategy. Such project revision has also involved a new definition of the control strategy, based on an over-speeding logic, and a suitable generator operational response was required, similarly as it was done in [13, 14].

In this work, the content of [15] has been extended with further steps regarding: (i) optimisation of the rotor, (ii) a new comparison with experiments performed on a small-scale hydro-turbine test model and (iii) numerical simulations of the coupled model of the hydro-turbine and PMG generator.

2 GEMSTAR system configuration and main characteristics

Fig. 1 shows the overall configuration of the GEMSTAR system with two turbines mounted on the two sides of a streamlined body through a connecting frame. Tail fins can be used in order to improve stability and dynamic response.

The floating body is tethered to the seabed through a flexible mooring cable. Such configuration is able to align to the current stream after the typical tidal direction changes. Moreover, the moored solution eliminates the need for a fixed underwater foundation, with possible benefits on the deployment and maintenance costs. The device can be, in fact, provided with a self-towing winch, which allows easier emersion and immersion manoeuvres, reducing the cost of maintenance operations. Different mooring solutions can be adopted. The simplest one comprises a single mooring line, as indicated in Fig. 2. A tailored control system which commands the turbines thrust (occasionally working as propellers) should be designed to avoid the 360° rotation of the system and the entanglement of the power cable.

In ordinary operations, the mooring cable is almost vertical, undergoing the effect of the support structure buoyancy. When subjected to a horizontal force, acting in presence of a water current, the mooring cable is tilted in an inclined position with a suitable angle, in order to ensure a sufficient clearance from the seabed in normal working conditions. The strategy to choose the cable tilt angle during operations must take into account a proper clearance from wave-induced motion and the optimal depth for maximum average water current speed.

Each rotor is coupled to an electric generator case in each of the side nacelles in Fig. 1. An inverter can be used for the connection to the electrical grid. Moreover, a suitable control logic can be implemented in order to track the optimal working conditions at different water current speeds, properly controlling the actual rotational speed and requested torque. The power connection is provided by means of a power cable, laid out along the mooring cable and extended up to an on-shore grid connection point.

A gearbox can be used to couple the turbine shaft to the generator rotor shaft, moving at significantly different rotational speeds.

It has to be noted that in the previous GEM system, a diffuser augmented (or shrouded) configuration was used, as described in [8]. The effect of the diffusers on turbine operation is described for example by Van Bussel [16] or by Reinecke *et al.* [17]. In the previously developed configuration, two annular diffusers were mounted around the turbines, with the aim to improve the energy conversion efficiency. This solution has been currently rejected based on two considerations: the cost of the added parts required and the expected large increase in the thrust acting on the turbines, according to previous analyses.

2.1 Previous studies on rotor hydrodynamic performance

After the design of the first-generation GEM configuration, different test campaigns were performed on the developed system, first on small-scale models then on a large-scale prototype.

The main test results in terms of power production performance can be reported using the non-dimensional power coefficient, defined as

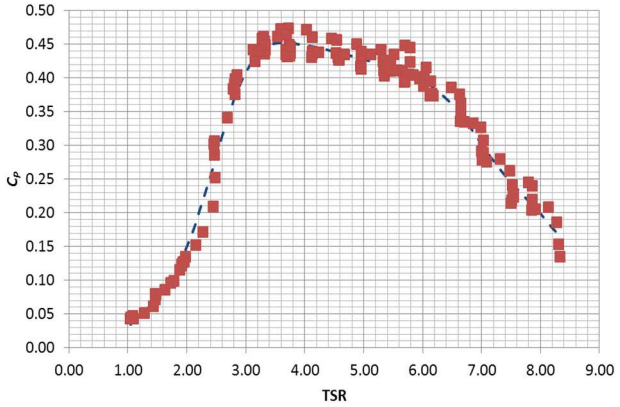

Fig. 3 *Power coefficient of a bare turbine mounted on the GEM floating system model (towing tank tests). Red dots are the experimental measurements and the dotted line represents cubic-spline fitting*

Fig. 4 *First GEM prototype on the dock*

Table 1 GEMSTAR first generation full-scale prototype (2012)

no. of rotors	2	overall weight	16,100 kg
rotor radius	1.5 m	overall width	10.4 m
nominal power (two rotors)	20 kW	overall length	9.2 m
power density (referred to turbine area)	1400 W/m^2	overall height	5.2 m

Table 2 Second generation GEMSTAR design parameters (2020)

no. of rotors	2	nominal current speed	2 m/s
rotor radius	6 m	cut-out current speed	3 m/s
nominal power (two rotors)	300 kW	expected power density	1300 W/m^2

$$C_P = \frac{P}{\frac{1}{2}\rho V^3 S} \tag{1}$$

where P is the mechanical power extracted by the turbine, V is the current velocity, S the reference surface (generally the rotor disk area) and ρ the water density. The power coefficient is generally reported as a function of another non-dimensional quantity, denoted as TSR (tip speed ratio), representing the blade tip speed normalised with respect to the flow velocity

$$\mathrm{TSR} = \frac{\omega R}{V} \tag{2}$$

where R is the rotor radius and ω is the rotational speed.

Some results of measured power coefficient for a small-scale turbine rotor (0.6 m diameter) are reported in Fig. 3. The reported data refer to a set of laboratory tests performed in the towing tank of the University of Naples on the model of the bare turbine of the old GEM configuration.

The maximum power coefficient is approximately equal to $C_P = 0.45$ and is reached at TSR = 4.0.

Comparable results were obtained in a set of sea tests on large prototype in the Venice Lagoon in 2012. A system with two turbines of 3 m diameter was deployed in a low-speed test site (with a maximum current speed of about 1.5 m/s). Fig. 4 shows the full-scale first generation prototype. Some details on the results of this campaign are given in [8] and the overall dimensions are summarised in Table 1.

It should be mentioned that all the structures have been designed for nominal total power of 100 kW for water speed of 2.6 m/s while the electrical generators nominal total power was set at 20 kW because the maximum speed at the chosen deployment site was 1.6 m/s.

The design objectives of the second generation GEMSTAR system are listed in Table 2.

The overall conversion efficiency from water current kinetic energy to electrical output has to account also for other sources of loss, due to the mechanical and electrical efficiencies. A further electromechanical efficiency, η, has to be applied to the hydrodynamic power coefficient in order to determine the effective power output

$$\eta = \eta_{\mathrm{m}}\eta_{\mathrm{e}} = 0.81 \tag{3}$$

where η_{m} and η_{e}, respectively, represent the mechanical and electrical losses.

Another important non-dimensional parameter is represented by the thrust coefficient, defined as

$$C_T = \frac{T}{\frac{1}{2}\rho V^2 S} \tag{4}$$

where T is the thrust acting on the rotor.

3 Rotor design

3.1 Definition of control strategy and related constraints

The cut-out speed defines the maximum water current speed at which normal power production is possible. A high cut-out speed, equal to the maximum expected current velocity of the deployment site, allows to exploit the whole available energy resource. Assuming a given size of the generator, a proper control strategy is needed in order to ensure that the generator operating limits are not exceeded.

Several control strategies can be assumed. In the present work, an over-speeding scheme was considered: the output power is kept at a constant value by reducing the required torque and increasing the rotational speed of the generator. Some details on this technique are provided by Zhou *et al.* in [13]. Using this approach, the generator will be operated in flux-weakening conditions.

A specific design of the blade is required in order to optimise the rotor performance, while complying with two operating requirements:

1. preventing excessive rotational speed (in order to limit the centrifugal forces, to avoid cavitation and to meet the generator rotational speed characteristics);
2. limiting the power and thrust increase above the rated conditions.

The effects of such constraints on blade design were investigated, imposing a maximum rotational speed equal to twice the rated speed and limiting the thrust and output power to their rated values.

The behaviour of tidal currents generally shows a relatively predictable pattern. Moreover, turbulent speed fluctuations are generally smaller in comparison to the atmospheric environment. These characteristics reduce the need for a very reactive control system, such as an active blade pitch control, as opposed to the

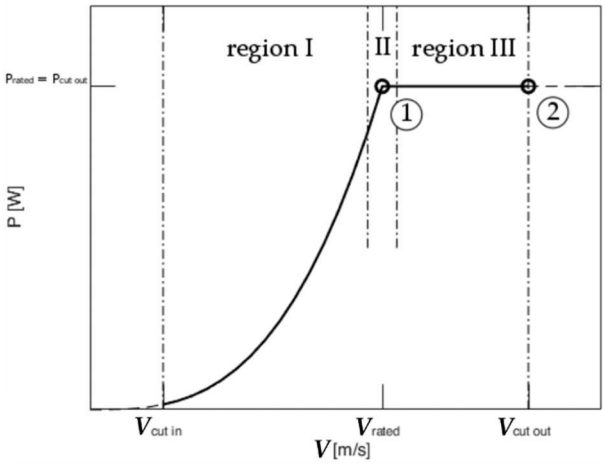

Fig. 5 *Ideal rotor power output curve, the circled numbers represent the two operating conditions, the other numbers represent the operating ranges. The power output increases as the cube of the stream speed in I, reaches the maximum value in II and it is kept constant in III*

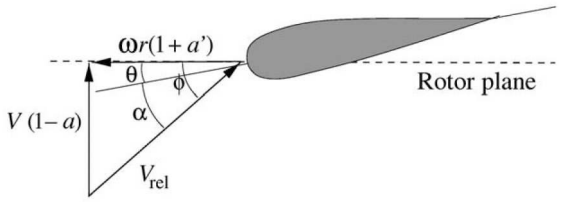

Fig. 6 *Relative velocity with axial and rotational inductions at a section of the rotor blade (reproduced from [18])*

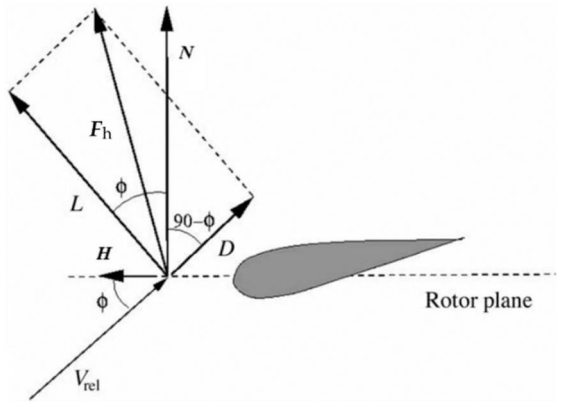

Fig. 7 *Hydrodynamic forces on a section and the normal and parallel projections with respect to the rotor plane (reproduced from [18])*

case of wind turbines. In this study, a fixed pitch configuration has been adopted, avoiding expensive moveable parts.

Power production is controlled by varying the rotational speed, tracking the power optimal conditions below the rated speed while limiting the output power above the rated speed. The rated flow speed is the water current speed at which the generator rated power is reached. Below the rated speed, the control system is designed to follow a constant TSR, corresponding to the maximum power coefficient, by increasing the rotational speed with increasing water stream velocity. In this region, the output power follows a typical cubic power trend for increasing flow speed. In the above rated region, the required torque is reduced and rotational speed is increased to keep a constant power value. Fig. 5 resumes the ideal required power curve showing the different regions of the control strategy.

3.2 Blade geometry definition

A design procedure was implemented in order to determine the main geometrical features of the blade, represented by twist and chord distributions. The design procedure is based on the objective to maintain constant power and thrust above the rated speed. Two operating conditions have been chosen, imposing that the corresponding values of thrust and power should be equal. The first operating condition (indicated as 1) is set at the rated water current speed, while the second one (indicated as 2) is fixed at the maximum current speed.

This constraint can be expressed in terms of the sectional thrust and power distribution along the blade span. Following the blade element momentum theory as in [18], one can express the sectional thrust and power as

$$\mathrm{d}T = \rho V^2 4a(1-a)\pi r\,\mathrm{d}r = \frac{1}{2}Nc\rho V_{\mathrm{rel}}^2 C_{\mathrm{N}}\,\mathrm{d}r \tag{5}$$

$$\mathrm{d}P = \rho V\omega^2 a'(1-a)4\pi r^3\,\mathrm{d}r = \omega\frac{1}{2}Nc\rho V_{\mathrm{rel}}^2 C_{\mathrm{H}} r\,\mathrm{d}r \tag{6}$$

where the symbols are explained in the nomenclature and a visual representation of the quantities is given in Figs. 6 and 7.

The proposed analytical procedure imposes equal sectional contributions at the two considered operating conditions, as indicated in the following relations:

$$\mathrm{d}T_1 = \mathrm{d}T_2 \tag{7}$$

$$\mathrm{d}P_1 = \mathrm{d}P_2 \tag{8}$$

Applying the actuator disk theory, (7) and (8) can be rewritten as

$$\rho V_1^2 4a_1(1-a_1)\pi r\,\mathrm{d}r = \rho V_2^2 4a_2(1-a_2)\pi r\,\mathrm{d}r \tag{9}$$

$$\rho V_1\omega_1^2 a_1'(1-a_1)4\pi r^3\,\mathrm{d}r = \rho V_2\omega_2^2 a_2'(1-a_2)4\pi r^3\,\mathrm{d}r \tag{10}$$

Equations (5) and (6) coupled with (9) and (10) can be solved to match the desired constraints, obtaining the unknown axial and rotational inductions and the sectional hydrodynamic coefficients.

The following system of equations is obtained:

$$V_1^2 8a_1(1-a_1)\pi r = N_B c V_{\mathrm{rel},1}^2(C_{l,1}\cos(\phi_1) + C_{d,1}\sin(\phi_1)) \tag{11}$$

$$V_1\omega_1^2 8a_1'(1-a_1)\pi r^2 = N_B c V_{\mathrm{rel},1}^2(C_{l,1}\sin(\phi_1) - C_{d,1}\cos(\phi_1)) \tag{12}$$

$$V_2^2 8a_2(1-a_2)\pi = N_B c V_{\mathrm{rel},2}^2(C_{l,2}\cos(\phi_2) + C_{d,2}\sin(\phi_2)) \tag{13}$$

$$V_2\omega_2^2 8a_2'(1-a_2)\pi r^2 = N_B c V_{\mathrm{rel},2}^2(C_{l,2}\sin(\phi_2) - C_{d,2}\cos(\phi_2)) \tag{14}$$

$$V_1^2 a_1(1-a_1) = V_2^2 a_2(1-a_2) \tag{15}$$

$$V_1\omega_1^2 a_1'(1-a_1) = V_2\omega_2^2 a_2'(1-a_2) \tag{16}$$

The system reported above contains the following variables:

- the induction factors, $a_1 a_1' a_2 a_2'$,
- the lift coefficients at the two chosen operating conditions.

The hydrodynamic coefficients of each blade section can be expressed as functions of the angle of attack or of the lift coefficient, $C_{\mathrm{l}}(\alpha)$ and $C_{\mathrm{d}}(C_{\mathrm{l}})$. A spline interpolant is used in the calculation, based on the results of the well-known Drela's aerodynamic software XFOIL [19].

A final relation should be added to the system of equation indicated above, relating the lift coefficients at the two chosen operational conditions:

$$C_{\mathrm{l},2} - C_{\mathrm{l},1} = C_{\mathrm{l}_\alpha}\Delta\alpha \tag{17}$$

The complete system of equations comprises seven equations in only six unknowns (four induction coefficients and two lift coefficients). To solve the problem a seventh unknown quantity should be added. In the adopted approach, the drag coefficient at

Table 3 Operating point conditions

Operating condition	Current speed, m/s	Rotor speed, rpm
1	2	16
2	3	32

Table 4 Rotor geometry

rotor radius	6 m	—	—
hub radius	0.6 m	—	—
no. of blades	3	—	—
chord distribution	Glauert's theory optimisation, design point 1	Glauert's theory optimisation design point 1 – chord increased	genetic algorithm optimisation
hydrofoil	EPPLER E818	—	—

Table 5 Performance of the turbine with the twist angle distribution modified by the algorithm

Operating condition	P analytical procedure	P WTPerf	T analytical procedure, kN	T WTPerf, kN
1	135.7 kW (C_P = 0.29)	127 kW (C_P = 0.27)	82.1	78
2	135.7 kW (C_P = 0.09)	166 kW (C_P = 0.11)	82.1	78.4

the second operating point has been assumed as the seventh variable. Later, one can try to match the resulting values of the drag coefficients through a proper choice of the hydrofoil sections.

Using a Newton–Raphson method, the system can be solved and the angle of attack $\alpha(C_l)$, which gives the desired lift coefficient, can be calculated. Knowing the angle of attack, α, and the inflow angle, ϕ, the required twist distribution along the blade, $\theta(r)$, can be determined as follows:

$$\theta(r) = \phi(r) - \alpha(r) \tag{18}$$

For validation purposes, the numerical code WTperf [20] has been used to estimate the performance of a rotor with the obtained chord distribution. The chord distribution is calculated through the Glauert's optimisation as in [18], choosing the first operating condition as the design point.

Due to the simplifications assumed in the analytical approach, some discrepancies between the results of the two analyses are expected. A single hydrofoil section along the blade was assumed in the analyses, considering a constant Reynolds number ($\mathrm{Re} = 5 \times 10^6$) for the evaluation of the hydrodynamic coefficients.

The design of the rotor blades must take into account the effects of cavitation. Such phenomenon consists in the generation of vapour bubbles when the local pressure of the fluid is lower than the vapour pressure, which is a function of the temperature for each given gas. To avoid the problems associated with cavitation, the expansion of the fluid on the blade has to be limited. A proper design of the hydrofoil can delay the occurrence of cavitation by limiting the peak of negative pressure coefficient on the suction side of the section. Initially, a hydrofoil specifically designed to avoid cavitation problems has been used, but the hydrodynamic characteristics of this hydrofoil did not allow to comply with the required constraints of constant power and thrust. Thus, an Eppler 818 hydrofoil, which shows a reduction in efficiency between the operating conditions 1 and 2 able to provide a steep reduction of power coefficient, was used for the analytical blade optimisation. The absence of cavitation on the blades, at the operating conditions 1 and 2, was checked after a first evaluation of the angles of attack seen by blade sections during operations. This was done assuming that the rotor tip is operating at a minimum depth of 5 m and the water temperature is 20°.

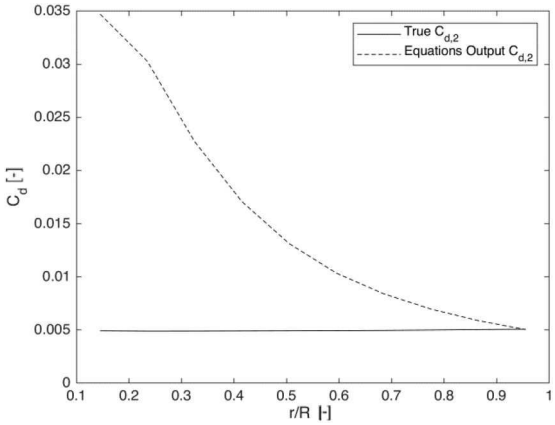

Fig. 8 *Sectional drag coefficient estimation at the second operating condition, as a function of the non-dimensional station radius r/R*

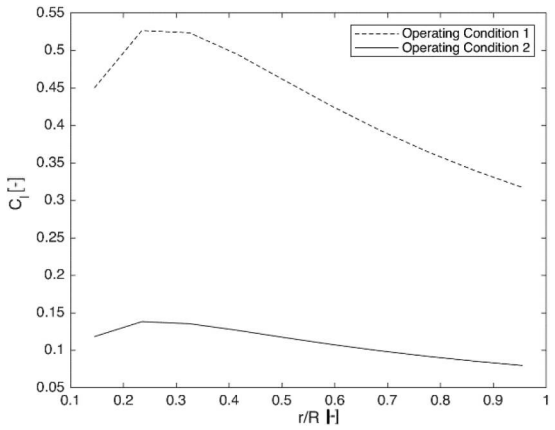

Fig. 9 *Sectional lift coefficient estimation at the two operating conditions*

Given the moderately low lift coefficients, minimum pressure coefficient was far off from the critical pressure coefficient, avoiding any effect of cavitation during operations.

An integration of cavitation check and hydrofoil shape optimisation is currently under development to better match the required design objectives. The operating conditions and the rotor geometry are summarised in Tables 3 and 4.

As stated above, the required C_d at condition 2 is one of the results of the analytical procedure, obtained by solving the equation system (11)–(17). Fig. 8 shows a comparison of the required and true drag coefficients at operating condition 2 along the blade.

In Fig. 8, the real C_d curve seems to show an almost constant trend due to a significant scale difference between the required and real coefficients and to the small variation of C_l along the blade, as indicated in Fig. 9, which reports the sectional lift coefficient along the blade span for the two operating conditions.

In Fig. 8, large differences between the desired and true drag coefficients can be observed, particularly in the inner part of the blade. In fact, difficulties have been observed in obtaining the desired performance. Table 5 reports the power and thrust values of the new rotor blade, estimated in the operating conditions 1 and 2, using both the simplified analytical procedure previously discussed and WTPerf.

As expected, the results of the analytical procedure and of WTPerf show significant differences, particularly with respect to the power predictions. The results of WTPerf show an ∼30% increase in power output from conditions 1 to condition 2, which can be related to the difference between the desired and real C_d. Moreover, WTperf accounts for some physical phenomena neglected in the simplified analytical procedure, such as, for example, Prandtl tip losses.

It can be further observed that, assuming the same chord distribution, the power output estimated using the twist distribution from the analytical procedure reaches an ∼40% lower value than

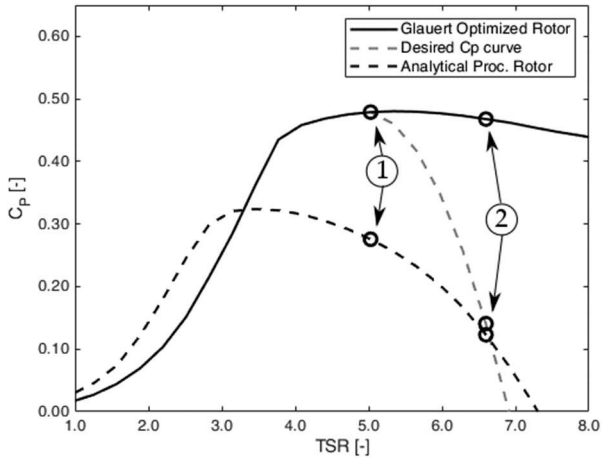

Fig. 10 *Power coefficient curves of the two rotors with different twist and the desired curve, with a sharp-decreased C_P after $C_{P,\max}$ (dashed line in grey), the circles represent the values corresponding to the first and second operating conditions*

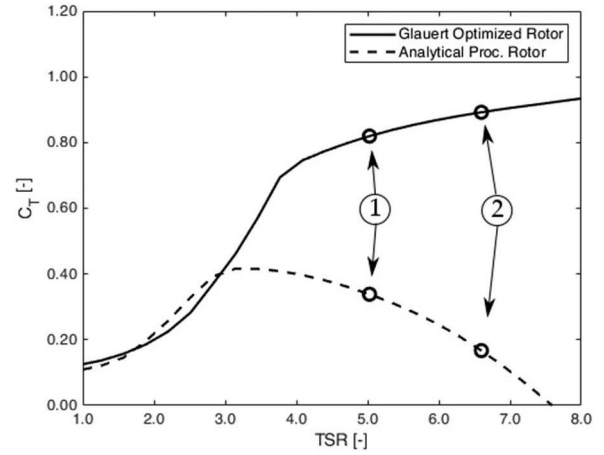

Fig. 11 *Thrust coefficient curves of the two rotors with different twist, the circles represent the values corresponding to the first and second operating conditions*

Table 6 Performance of the turbine with the twist angle distribution modified by the algorithm and chord distribution increased by 50%

Operating condition	P analytical procedure	P WTPerf	T analytical procedure, kN	T WTPerf, kN
1	164.2 kW (C_P = 0.35)	152.4 kW (C_P = 0.33)	103.9	98.0
2	164.2 kW (C_P = 0.11)	186.7 kW (C_P = 0.12)	103.9	98.0

the power output for a twist distribution optimised according to Glauert's theory.

Figs. 10 and 11 show a comparison of the power and thrust coefficients for the rotor determined with the analytical procedure and the rotor optimised with Glauert's theory. The latter C_P curve reaches a larger peak value, but is unsuitable to limit output power in condition 2 as requested.

The curves of thrust and power coefficients, determined using the rotor twist from the analytical procedure, show lower peak values, but the steeper negative slopes observed above the peak points allow a reduction of thrust and power values at condition 2, consistent with the optimisation goal.

A modification of the chord distribution can improve power performance for the same twist distribution. A first attempt with a 50% increased chord yielded a 20% increase in power and 25% increase in thrust. The results related to the adjusted chord

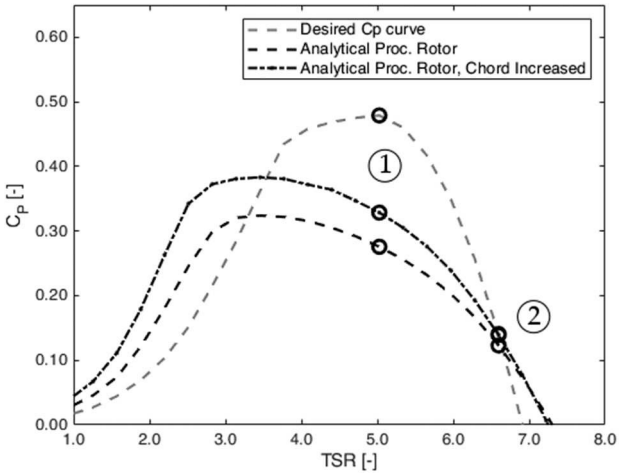

Fig. 12 *Power coefficient curves of the two rotors with different chord and the desired curve (dashed line in grey), the circles represent the values corresponding to the first and second operating conditions*

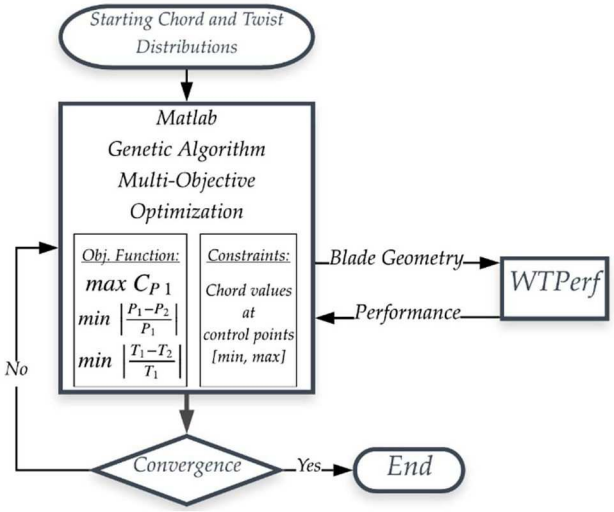

Fig. 13 *Flow-chart of the optimisation tool with the integration of the Matlab© genetic algorithm and WTPerf*

configuration are reported in Table 6. The power coefficient at condition 1 is, however, lower than the desired value, as shown in Fig. 12.

3.3 Blade geometry optimisation

A different approach to the shape optimisation problem has been also considered, in order to properly account for the effects of both chord and twist distributions simultaneously. A multi-objective genetic algorithm, available in the Matlab© Optimisation Toolbox [21], was used to search for the optimal chord and twist, using WTPerf to evaluate the performance of each individual rotor. A scheme of the optimisation procedure is reported in Fig. 13.

The design space was defined by the chords and twists at five stations along the blade. A piecewise cubic interpolation was used to reconstruct the geometrical characteristics at each intermediate section.

Three parameters were used in the definition of the multi-objective function:

- mechanical output power at operating condition 1;
- the difference between output power at the two operating condition chosen;
- the thrust difference between the two conditions.

A theoretical background for the genetic algorithm tool can be found in [21]. The algorithm creates a sequence of generations. Each generation comprises 200 individuals, which represent

Table 7 Performance of the turbine with the twist angle distribution modified by the genetic optimisation algorithm

Operating condition	P WTPerf	T WTPerf, kN
1	149.0 kW (C_p = 0.32)	100.0
2	146.4 kW (C_p = 0.09)	99.7

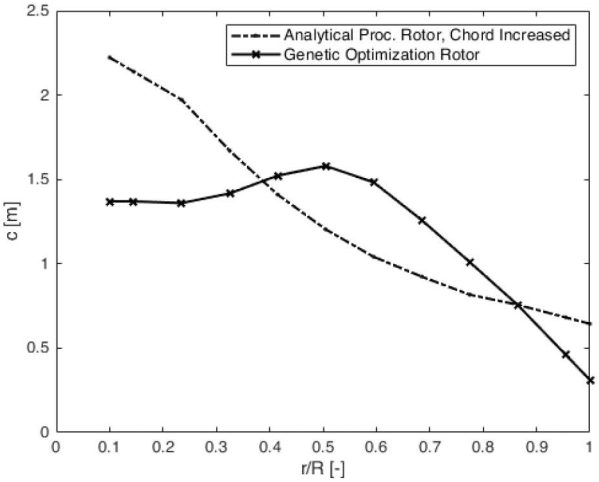

Fig. 14 *Comparison between the chord distribution used in the analytical procedure and the one obtained through the optimisation tool*

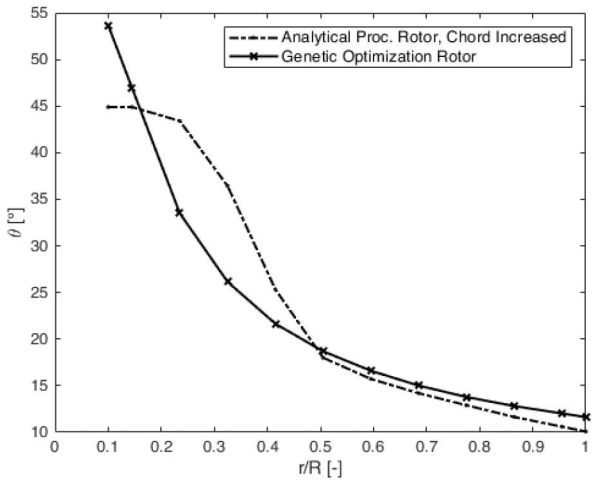

Fig. 15 *Comparison between the twist distribution obtained through the analytical procedure and the one obtained through the optimisation tool*

different rotor geometries. The convergence criterion is based on the average distance, named 'spread', among selected individuals of two consecutive generations. In the performed numerical test, convergence was reached after 118 generations.

Table 7 illustrates the performance of the individual with higher output power at operating condition 1 and with thrust and power variations between the two operating conditions lower than 5%.

The chord and twist distributions for the rotor geometry determined through the optimisation tool are reported in Figs. 14 and 15, in comparison to the chords and twists used in the analytical procedure. A comparison of the power coefficients to the desired values and to the results of the analytical procedure is reported in Fig. 16, while Fig. 17 reports a comparison of the thrust coefficients.

Despite the difference in chord and twist distributions, the curves of C_P and C_T from the genetic optimisation and from the analytical procedure show similar trends. The two approaches yield similar results for the output power, suggesting that a further improvement of power performance requires a specific hydrofoil shape design.

To improve the overall performance of the turbine, an attempt was carried out to release the constraints on the second operating

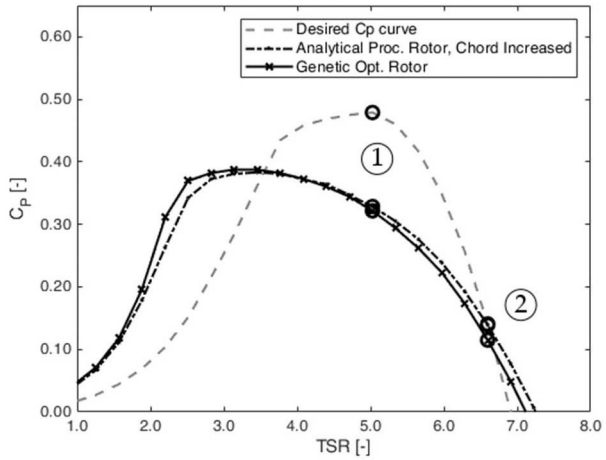

Fig. 16 *Power coefficient curves of the two rotors with different design approach and the desired curve (dashed line in grey); the circles represent the values corresponding to the first and second operating conditions*

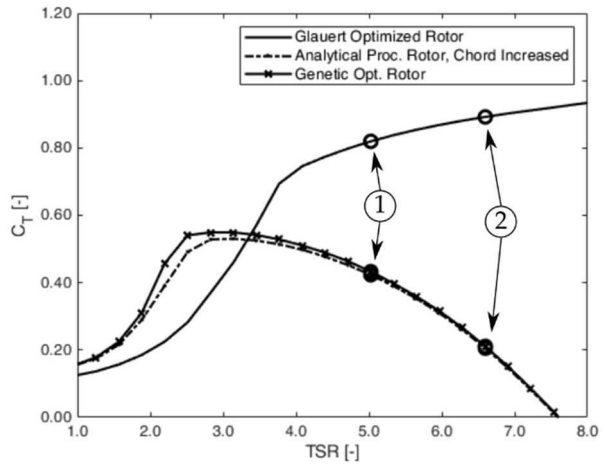

Fig. 17 *Thrust coefficient curves corresponding to the rotors obtained with the two design approaches and to the Glauert optimised rotor; the circles represent the values corresponding to the first and second operating conditions*

condition of rotor speeds. The aim, in fact, was to move the maximum power coefficient towards the rated current speed, in order to enhance the extraction of energy. The analytical procedure was used to get a first evaluation of the maximum power coefficient designing the rotor with a different set of inputs of operating conditions. The new operating condition is indicated as condition ②' in Figs. 18 and 19. We got a first estimation of how much we had to increase the TSR at ② to obtain a satisfactory value of power coefficient at ①.

The new rotor speed, at the second operating condition, was increased by 15%. This constraint must be carefully analysed during the coupling process with an electrical generator, in particular a higher rotor speed would imply a properly sized generator. With this assumption, the genetic optimisation procedure yielded a new blade shape, resulting in a higher power coefficient at the first operating condition and a consequent increment of the thrust coefficient, as shown in Figs. 18 and 19.

The improved blades design obtained through the genetic optimisation was used in a scaled-model 3D printed hydro-turbine rotor and this was tested in the towing tank of the University of Naples. The turbine was installed on a torque motor/generator equipped with a torque meter and three load cells to measure the rotor in-plane forces and the axial force. Varying the rotational speed of the turbine, with a constant carriage speed, the rotor performance at a wide range of tip speed ratios was measured. To analyse the same range of tip speed ratios of the full scale turbine, the rotational speed was increased according to the scale of 1:30, obtaining the test conditions listed in Table 8.

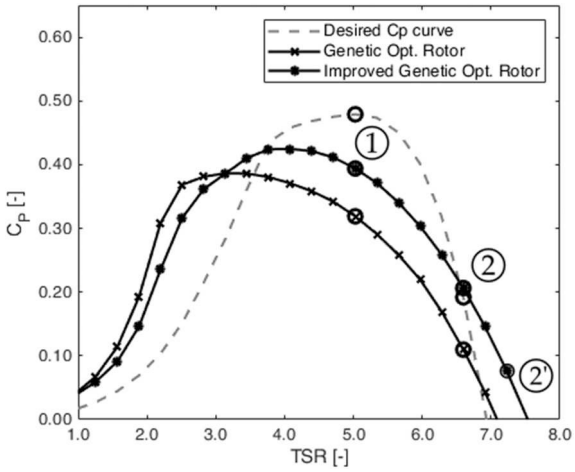

Fig. 18 *Power coefficient curves of the two rotors optimised through the genetic algorithm and the desired curve (dashed line in grey); the circles represent the values corresponding to the first, the second and the new operating conditions*

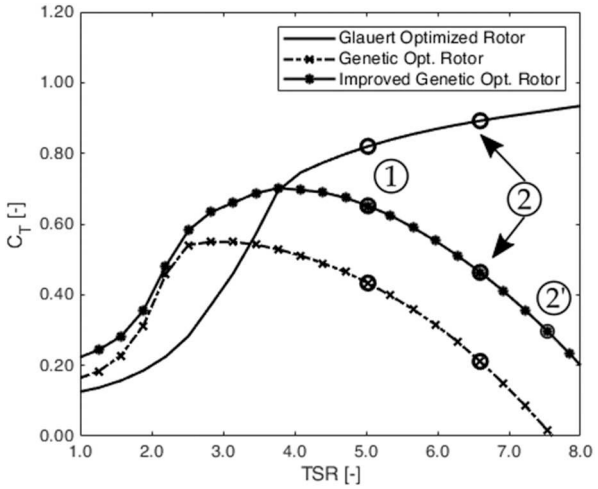

Fig. 19 *Thrust coefficient curves corresponding to the optimised through the genetic algorithm and to the Glauert optimised rotor; the circles represent the values corresponding to the first, the second and the new operating conditions*

Table 8 Test conditions of the scaled model hydro-turbine

Characteristics	Test model
scale	1:30
carriage speed	1.2 m/s
rotor speed	from 20 RPM to 320 RPM
water temperature	25°
blade sections	EPPLER 818 16% thickness

Due to the different scale of the tested configuration, the rotor performance experimental values have been compared to a different set of numerical values obtained from WTPerf code. It is worth to specify that the chosen section hydrofoil (Eppler 818) thickness has been increased to 16% t/c due to a measured excessive bending of the 3D printed blades with the original geometry. 2D hydrodynamic coefficients of the chosen hydrofoil were then calculated using the appropriate Reynolds number ($\mathrm{Re} = 1 \times 10^5$). Fig. 20 shows a comparison between the power coefficient curve calculated with the numerical model for the full scale rotor and for the model scale rotor and the mean values measured during the experimental test on the 3D printed model. The decrement in maximum power coefficient between the real scale and the model scale curve is mainly due to the reduction of the local blade sections Reynolds number as mentioned before. To account for the high roughness of the 3D printed turbine, in the

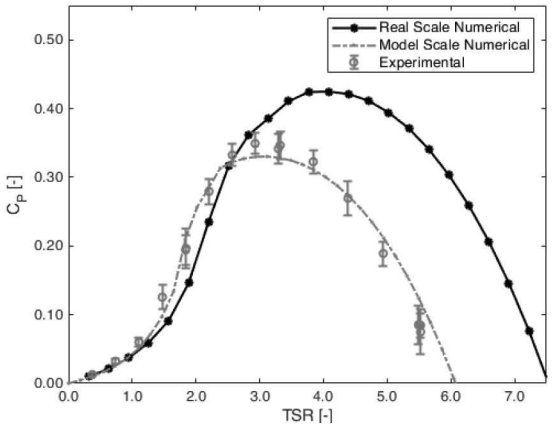

Fig. 20 *Comparison between numerical and experimental power coefficient of the rotor optimised through the genetic algorithm; the black starred-line refers to the real scale values; the grey dashed-line refers to the numerical model scale values and the grey circles to the mean experimental values; the error-bars lengths are equal to two times the standard deviation of the measurements for each tip speed ratio*

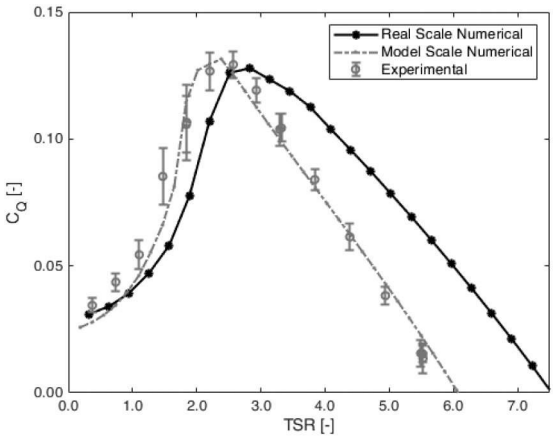

Fig. 21 *Comparison between numerical and experimental torque coefficient curves of the rotor optimised through the genetic algorithm; the black starred-line refers to the real scale values; the grey dashed-line refers to the numerical model scale values and the grey circles to the mean experimental values; the error-bars lengths are equal to two times the standard deviation of the measurements for each tip speed ratio*

model-scale numerical model, the 2D hydro-dynamic coefficients extracted through XFOIL have been obtained imposing leading-edge turbulent transition.

The real-scale numerical C_Q–TSR curve (shown in Fig. 21) has been used to get an estimation of the actual mechanical torque that the real size hydro-turbine would transmit to the electrical generator. A look-up table of the mechanical torque as a function of the current speed and the rotor speed $Q(V, \omega)$ produced by the hydro-turbine has been calculated through the following formula:

$$Q = \frac{1}{2}\rho V^2 S R\, C_Q(\mathrm{TSR}) \tag{19}$$

where the torque coefficient has been extracted from the numerical curve and S and R represented the geometry of the real-scale rotor. A simulation model of the coupling between the turbine and the electrical generator was carried out to evaluate the behaviour of the overall system.

4 Control of the turbine electrical generator

The performance of the electrical generator is crucial for power extraction maximisation and losses reduction. It is strictly related to the turbine adopted in the application. In fact, the use of an adjustable pitch turbine causes the angular speed of the turbine to be practically kept constant, while speed variation is very low.

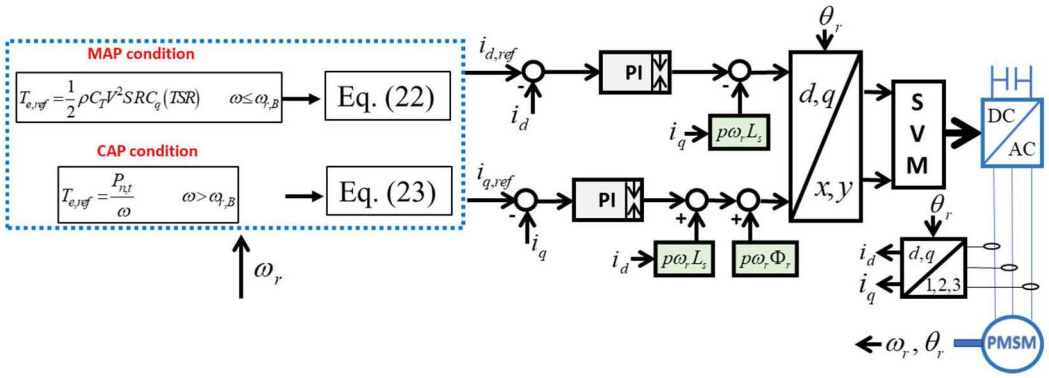

Fig. 22 *Control scheme for the electrical generator*

Consequently, the electrical generator works in a fixed speed point, so determining good advantages in terms of iron losses reduction. On the other hand, the use of non-controllable pitch turbine to maximise power extraction leads to a large variation of angular rotor speed, which results in the need of improved control of the electrical generator. In this latter case, the rated angular speed of the generator is often overtaken, so a proper control method must be considered to optimise the generator behaviour in the flux weakening region [13], by also accomplishing with the suitable used machine [22, 23]. In the presented paper, the superficial permanent magnet machine is considered. As well known from the literature, the control approach is usually based on the maximum torque per ampere algorithm (MTPA). The rotor reference frame model can be expressed as follows:

$$\begin{cases} v_d = R_\mathrm{s} i_d + L_\mathrm{s}\dfrac{\mathrm{d}\, i_d}{\mathrm{d}t} - p\,\omega_\mathrm{r} L_\mathrm{s} i_q \\ v_q = R_\mathrm{s} i_q + L_\mathrm{s}\dfrac{\mathrm{d}\, i_q}{\mathrm{d}t} + p\omega_\mathrm{r} L_\mathrm{s} i_d + p\,\omega_\mathrm{r}\Phi_\mathrm{r} \\ T_\mathrm{r} - T_\mathrm{e} = J\dfrac{\mathrm{d}\,\omega_\mathrm{r}}{\mathrm{d}t} \\ T_\mathrm{e} = \dfrac{3}{2} p\,\Phi_\mathrm{r} i_q \end{cases} \tag{20}$$

The d–q-axis voltages and the currents must be chosen in order to verify that $v_d^2 + v_q^2 \le V_L^2$ and $i_d^2 + i_q^2 \le I_L^2$.

The adopted control scheme is shown in Fig. 22, and it is inherent the power control of the electrical generator. The shaft of the generator is coupled with the turbine through a mechanical gear. The main idea of the proposed control is that the angular speed of the generator follows the turbine angular speed (opportunely reported to the shaft of the electrical generator with the mechanical gear ratio), and in this way, the torque of the generator can be opportunely controlled. The control on the torque guarantees to extract the power available from the turbine, addressing a maximum active power (MAP) and a constant active power (CAP) control zone, as shown in the control scheme depicted in Fig. 22. Starting from the value of the generator angular speed, it is possible to determine the torque reference with the following relations:

$$\begin{cases} T_{\mathrm{e,ref},1} = \dfrac{1}{2}\rho\, C_\mathrm{T} V^2 S\, R\, C_q(\mathrm{TSR}) \quad \omega \le \omega_{\mathrm{r},B} \\ T_{\mathrm{e,ref},2} = \dfrac{P_{n,t}}{\omega} \quad \omega > \omega_{\mathrm{r},B} \end{cases} \tag{21}$$

When the angular speed of the generator is below the base speed, the torque is calculated using the map of the turbine obtained with (19); while in overspeed condition, the power of the generator must be limited to the rated power of the turbine and the reference torque is easily obtained though the angular speed.

From the reference value of torque and using the MTPA algorithm [22], [23], the value of direct current i_d is fixed to zero until the angular speed is below the based speed, while the reference of quadrature axis current can be obtained directly from the torque reference

$$\begin{cases} i_{d,\mathrm{ref}} = 0 \\ i_{q,\mathrm{ref}} = \dfrac{2T_{\mathrm{e,ref},1}}{3p\,\Phi_\mathrm{r}} \end{cases} \tag{22}$$

When the speed overcomes the based speed, the direct and quadrature axis current assume a suitable value according to the following formula:

$$\begin{cases} i_{d,\mathrm{ref}} = \sqrt{\left(\dfrac{V_\mathrm{n}}{p\omega_\mathrm{r} L_\mathrm{s}}\right)^2 - i_{q,\mathrm{ref}}^2} - \left(\dfrac{\Phi_\mathrm{r}}{L_\mathrm{s}}\right) \\ i_{q,\mathrm{ref}} = \dfrac{2T_{\mathrm{e,ref},2}}{3p\,\Phi_\mathrm{r}} \end{cases} \tag{23}$$

The absolute value of $i_{d,\mathrm{ref}}$ grows with the increase of angular speed, while its maximum value is limited by the constraint of demagnetisation, the maximum angular speed and the current limit. The utilised formula permits to limit the amount of total electrical power, respecting the rated machine power. In addition, the constant power range must be guaranteed during the long performance of the turbine also in case when occurs an overloaded for a short time duration due to a sudden sea current fluctuation on the turbine.

The saturation limits for the direct and quadrature axis are defined by considering the operating point of the machine and choosing an appropriate value of limit current for the electrical drives. For the direct axis, the upper limit is fixed to zero, while the lower limit is determined by the demagnetisation limit of the machine ($i_{d,\max} = \Phi_\mathrm{r}/L_\mathrm{s}$).

5 Numerical results

In order to verify the goodness of the proposed control technique, a set of current speed data was obtained through the software TurbSim from NREL, which employs a semi-empirical method to simulate a turbulent speed time-history. The software allows the user to choose the mean speed and the turbulence level. In this case study, the mean speed is the rated current speed of the turbine and the turbulence level is equal to that of the tidal current experimental data extracted during a measurement campaign in the Strait of Messina, Italy, and it has been set at 10%. The time duration of the tidal current adopted in the simulation is fixed at 600 s and the utilised sample rate is 1 S/s.

Table 9 reports the main parameters of the electrical generator.

The rated active power of the electrical generator has been chosen equal to the maximum power of the turbine, both for a reduction of cost and in order to guarantee that the performance in the range 140–150 kW reaches the highest efficiency values. Considering the rated angular speed of the turbine (i.e. 16 rpm) and the rated speed of the generator, a mechanical gear with a ratio of 1:100 is used for the coupling between the turbine and the electrical generator. In the simulation environment, the behaviour of the mechanical gear is considered ideal (i.e. the losses and the

Table 9 Electrical generator main parameters

Electrical generator parameters	
rated active power	150 kW
DC-link voltage	600 V
limit current (rms), I_L	300 A
rated angular speed, $\omega_{r,n}$	1600 rpm
poles pairs, p	4
rotor flux, Φ_r	0,35 Wb
R_s	0,05 Ω
L_s	0.8 mH
inertia, J	0. 5 kgm^2

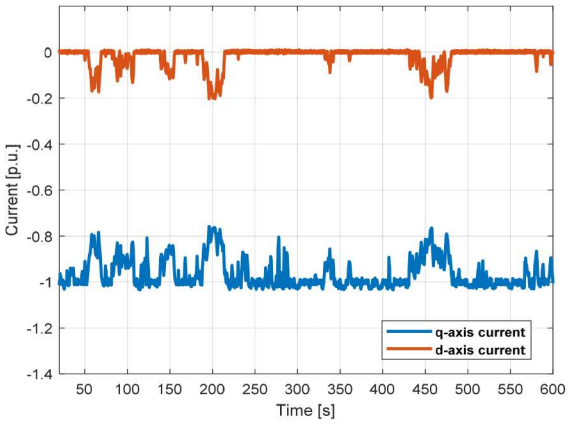

Fig. 23 *Time behaviour of d-axis current (red line above) and q-axis current (blue line below) for the constant mean current speed case*

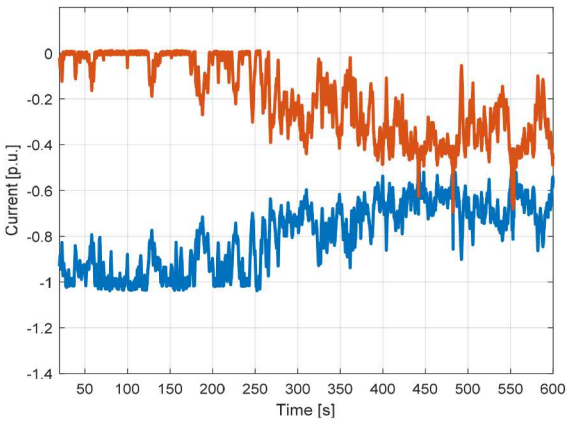

Fig. 24 *Time behaviour of d-axis current (red line above) and q-axis current (blue line below) for the current speed ramp case*

effect on the dynamics are neglected). The adopted power circuit is an IGBT six-step inverter with a modulation frequency of 5 kHz.

Two different simulations are reported in the paper. The first is related to a case with constant mean speed with the assumed turbulence intensity, the latter shows a case study with the tidal current ramping from 2 to 3 m/s in the interval from 180 to 420 s superimposed to the same turbulence model, conservatively assuming the same turbulence intensity at each speed. The time behaviours of d–q-axis current are reported in Figs. 23 and 24, where the zoom in the range 20–600 s is considered. As it can be seen, the q-axis current varies around 0.75–1 p.u. in the first case and 0.41–1 p.u. in the second case; while the d-axis current reaches the maximum value of 0.2 p.u. in the constant mean speed case, instead has a maximum value of 0.69 p.u. for the current speed ramp case. This is due to the fact that the maximum speed of the tidal current is about 3.6 m/s, and the angular speed of the generator exceeds the rated speed. This condition forces the generator to work in the flux weakening region, limiting the generated electrical power.

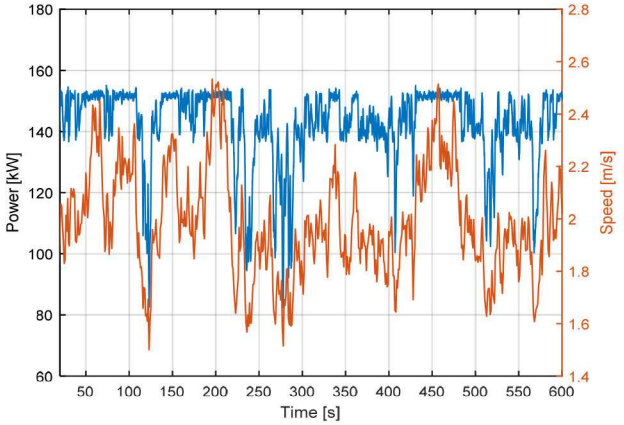

Fig. 25 *Generated active power (kW) (blue line above) and speed of the tidal current (m/s) (red line below) for constant mean current speed input*

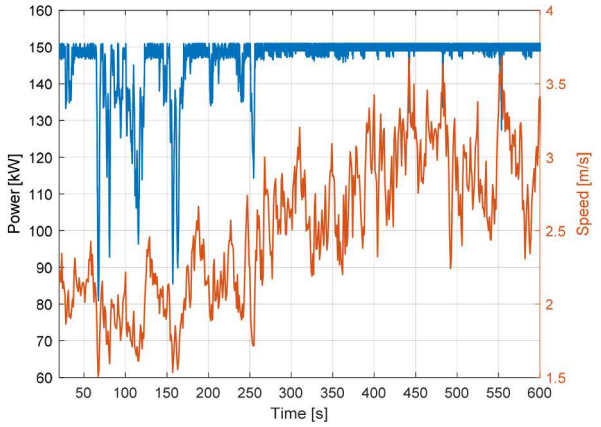

Fig. 26 *Generated active power (kW) (blue line above) and speed of the tidal current (m/s) (red line below) for the current speed ramp case*

The electric active powers, obtained by neglecting the iron losses in the generator, are reported in Figs. 25 and 26.

The large CAP generation identifies the working points where the rated speed of the generator is reached and/or is surpassed, with the necessity of the flux weakening. The reported trends obviously show that the variation of electric active power is strictly linked to the tidal stream speed time history and the proposed control allows to correctly follow these current speed variations. As it is possible to note, the rated active power of the generator is reached for a tidal speed of at least 2 m/s, according to the design of the turbine. The hydrodynamic performance of the turbine is shown in the following figures for the two simulated cases.

As it can be noticed from Fig. 27, a value of the hydrodynamic power coefficient close to the optimal design value of about 0.42 is reached in the constant mean current speed at 2 m/s simulation. The thrust coefficient is nearly constant in this case, as well as the TSR.

On the other hand, as shown in Fig. 28, as the mean current speed is increased to a value of 3 m/s, the power coefficient reduces accordingly to a lower mean value, cooperating with the flux weakening control in limiting the generated electric power. Moreover it can be observed that, according to the design goals illustrated in Section 3, the thrust coefficient reduces to lower values for increasing values of TSR.

It is worth mentioning that even if the turbulence intensity level is constant in both simulations (10%), higher oscillations of power and thrust coefficients can be observed in the current speed ramp case for higher mean current speed. This is due to the fact that the slopes of C_P–TSR and C_T–TSR curves are higher in the TSR ranges corresponding to high current speed operating conditions.

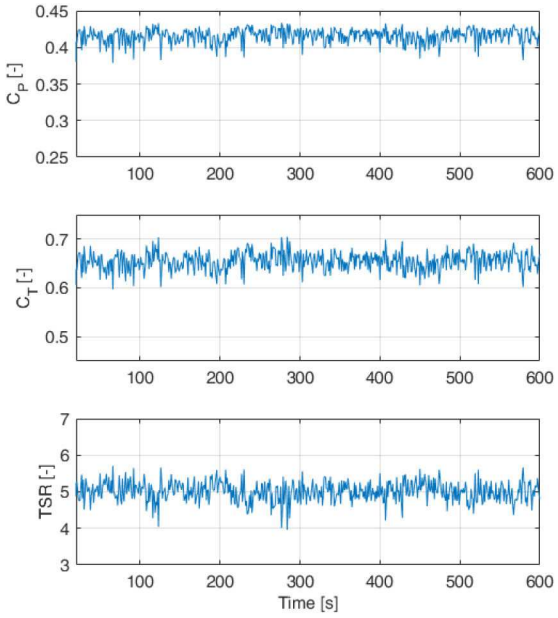

Fig. 27 *Simulated time histories of hydrodynamic power coefficient (upper), hydrodynamic thrust coefficient (middle), tip speed ratio (lower) for the constant mean current speed case*

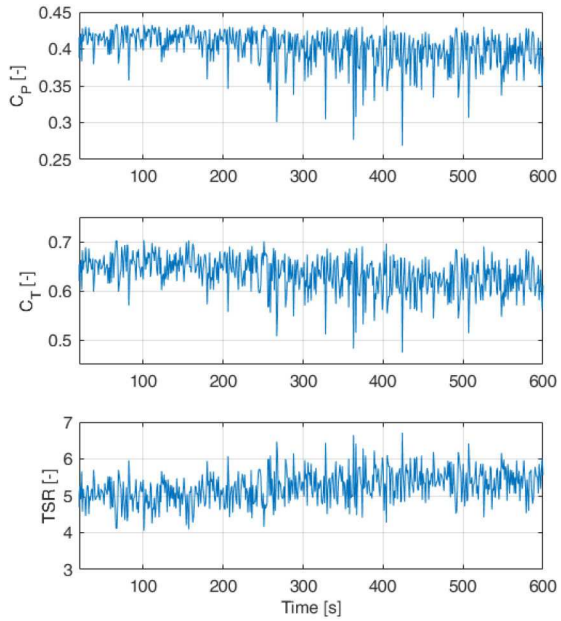

Fig. 28 *Simulated time histories of hydrodynamic power coefficient (upper), hydrodynamic thrust coefficient (middle), tip speed ratio (lower) for the current speed ramp case*

6 Conclusions

Two main aspects of a hydrokinetic turbine design were presented: hydrodynamic design and generator control. After a description of the main characteristic of the GEMSTAR project, a procedure for the redesign of the turbine blade was described, with the objective to comply with the requirement of constant power and thrust above the rated speed. The performed study leads to a revision of the chord and twists distributions and highlighted the need for a specific hydrofoil shape design.

Finally, an analysis of the generator electric control was presented through the definition of a numerical model. The developed control system is designed for a fixed pitch turbine using an over-speeding control strategy. This solution requires a specific attention to the generator behaviour in the flux-weakening region. Therefore, a set of simulations was carried out by considering a tidal current profile obtained through the software TurbSim and by using the main characteristics of the designed turbine. In order to prove the effectiveness of the proposed control strategy, two different tidal current conditions, in which over-speeding conditions were repeating frequently, have been considered. The obtained results highlighted the good dynamic behaviour of the electrical generator control, both in the MAP and in CAP mode.

7 References

[1] Magagna, D., Margheritini, L., Alessi, A., *et al.*: '*Workshop on identification of future emerging technologies in the ocean energy sector*' (European Commission, Luxembourg, 2018)

[2] Simec Atlantis Energy: 'Turbines'. Available at https://simecatlantis.com/services/turbines/. [Accessed 26 06 2020]

[3] Zhou, Z., Benbouzid, M., Charpentier, J.-F., *et al.*: 'Developments in large marine current turbine technologies – a review', *Renew. Sust. Energy Rev.*, 2017, **71**, pp. 852–858

[4] Orbital: 'Orbital marine O2'. Available at https://orbitalmarine.com/orbital-o2. [Accessed 25 05 2020]

[5] Minesto: 'Minesto technology'. Available at: https://minesto.com/our-technology. [Accessed 25 06 2020]

[6] Shirasawa, K., Minami, J., Shintake, T.: 'Scale-model experiments for the surface wave influence on a submerged floating ocean-current turbine', *Energies*, 2017, **10**, p. 17

[7] Corporation, I.H.I.: 'IHI demonstrated the world's largest ocean current turbine for the first time in the world', *IHI Eng. Rev.*, 2019, **52**, (1), p. 2B

[8] Coiro, D.P., Troise, G., Scherillo, F.: 'Design, towing tank test and deployment of full scale GEM, a novel tethered system for harnessing tidal energy'. Proc. of Asian Wave and Tidal Energy Conf. (AWTEC 2012), Jeju (South Corea), 2012

[9] Vikas, M., Rao, S., Seelam, J.K.: 'Tidal energy: a review'. Proc. of Int. Conf. on Hydraulics, Water Resources and Coastal Engineering (Hydro2016), Pune, India, 2016

[10] Roberts, A., Thomas, B., Sewell, P., *et al.*: 'Current tidal power technologies and their suitability for applications in coastal and marine areas', *J. Ocean Eng. Mar. Energy*, 2016, **2**, pp. 227–245

[11] Coiro, D., Troise, P.G., Ciuffardi, C., *et al.*: 'Tidal current energy resource assessment: the strait of Messina test case'. Int. Conf. on Clean Electrical Power: Renewable Energy Resources Impact, Alghero, Italy, 2013, DOI: 10.1109/ICCEP.2013.6586992

[12] Winter, A., Tryfonas, T.: 'A constrained optimisation process for the design of tidal turbine blades with experimental validation'. OCEANS'11 MTS/IEEE KONA, Waikoloa, HI, USA, 2011

[13] Zhou, Z., Scuiller, F., Charpentier, J.F., *et al.* 'Power control of a nonpitchable PMSG-based marine current turbine at overrated current speed with flux-weakening strategy', *IEEE J. Ocean. Eng.*, 2015, **40**, (3), pp. 536–545

[14] Winter, A.: 'Speed regulated operation for tidal turbines with fixed pitch rotors'. OCEANS'11 MTS/IEEE KONA, Waikoloa, HI, USA, 2011

[15] Coiro, D.P., Iannuzzi, D., Coppola, M., *et al.*: 'Coupling fixed pitch rotor design to PMG de-fluxing control for GEMSTAR marine current turbine'. Proc. of 2019 Int. Conf. on Clean Electrical Power (ICCEP), Otranto, Italy, 2019

[16] Van Bussel, G.J.: 'The science of making more torque from wind: diffuser experiments and theory revisited', *J. Phys.: Conf. Ser.*, 2007, **75**, pp. 1–12, 2111

[17] Reinecke, J., Von Backstrom, T., Venter, G.: 'Effect of a diffuser on the performance of an ocean current turbine'. 9th European Wave and Tidal Energy Conf. (EWTEC), University of Southampton, Southampton, UK, 2011

[18] Hansen, M.O.L.: '*Aerodynamics of wind turbines*' (Earthscan, London, 2008)

[19] Drela, M.: 'XFOIL: an analysis and design system for low reynolds number airfoils'. Proc. of the Conf. Low Reynolds Number Aerodynamics, Notre Dame, Indiana, USA, 1989

[20] Platt, A.D., Buhl, Jr. M.L.: '*WT_perf user guide for version 3.05.00*' (NREL National Renewable Energy Laboratory, Golden, CO, 2012)

[21] MathWorks: 'Matlab R2018b documentation', MathWorks, 2018. Available at https://it.mathworks.com/help/gads/gamultiobj.html. [Accessed 14 January 2019]

[22] Dong, Z., Yu, Y., Li, W., *et al.*: 'Flux-weakening control for induction motor in voltage extension region: torque analysis and dynamic performance improvement', *IEEE Trans. Ind. Electron.*, 2018, **65**, (5), pp. 3740–3751

[23] Liu, C.G., Han, Z., Yu, H.: 'IPMSM model predictive control in flux-weakening operation using an improved algorithm', *IEEE Trans. Ind. Electron.*, 2018, **65**, (12), pp. 9378–9387